Journal of Materials Chemistry A

Accepted Manuscript

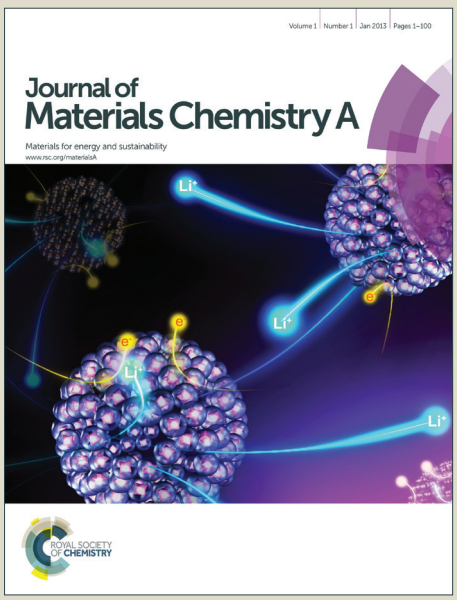

ROYAL SOCIETY OF CHEMISTRY

www.rsc.org/materialsA

Cite this: DOI: 10.1039/c0xx00000x

www.rsc.org/xxxxxx

ARTICLE TYPE

"Nano to nano" electrodeposition of WO_3 crystalline nanoparticles for electrochromic coatings†‡

Liang Liu[a,b], Michael Layani[a], Shai Yellinek[a], Alexander Kamyshny[a], Han Ling[b], Pooi See Lee[b], Shlomo Magdassi*[a] and Daniel Mandler*[a]

Received (in XXX, XXX) Xth XXXXXXXXX 20XX, Accepted Xth XXXXXXXXX 20XX
DOI: 10.1039/b000000x

A "nano to nano" electrodeposition approach for preparing nano-structured thin films from the dispersion of nano-objects is reported. A typical WO_3 system is demonstrated, where nanocrystalline films are electrodeposited onto transparent conductive electrodes such as ITO and Ag grid printed PET (Ag grid/PET) from the water dispersion of WO_3 nanoparticles without applying high potential, adding surfactants or polymers. The process is based on the reduction of WO_3, which eliminates the electrostatic repulsion between the nanoparticles causing film deposition on the cathode. The reduced WO_3 (HWO_3) is conductive, thus it allows further film growth towards higher thickness and coverage. The electrodeposited films consist of stacked crystalline nanoparticles, which provide high active surface area, facilitate the penetration of electrolyte and the intercalation/deintercalation of Li^+ in the nanocrystals and therefore result in outstanding electrochromic performance and stability (92% contrast, 9 s coloring and 15 s bleaching, retaining 76% contrast after 1000 coloring/bleaching cycles). The thickness, electrochromic performance and surface coverage of the films are well tuned by potential and time. This novel "nano to nano" electrodeposition approach based on the electrochemical redox of nano-objects can be extended to various transition metal oxide nano-objects with different size and shape.

Introduction

The synthesis of nanostructured materials, *e.g.* nanoparticles, nanorods and nanotubes, has matured and reached a level where their structure, size and complexity can be well-controlled[1, 2]. It has been shown that nanostructured materials have superior performance in various applications as compared with bulk materials. For many of these applications thin films are highly desired. The latter are usually deposited either from the gaseous phase, such as by chemical vapor deposition, or from the liquid phase, *e.g. via* dip- or spin-coating. Wet deposition of nanomaterials is performed while using dispersions, in which aggregation of the particles is prevented by electrostatic or steric stabilization mechanism. The most common methods for depositing thin nanostructured films, *i.e.* spin-, dip- and cast-coating are usually limited to flat surfaces and the control of the thickness is difficult. Electrodeposition, on the other hand, is very useful for coating complex geometries and enables well controlling the film thickness. Commonly, electrodeposition of nanomaterials comprises the "bottom-up" approach where molecular species, *e.g.* metal ions, are oxidized or reduced and deposited (due to the low solubility of the product) to form typically bulk material[3-5]. To form nanostructured films electrochemically from molecular species, it is necessary to add surfactants or polymers, which tend to remain in the film deteriorating its performance[6, 7]. Nanostructured films can also be deposited starting with dispersions of nano-objects. Electrophoretic deposition is well established and enables deposition of charged nano-objects especially nanoparticles; however requires very high voltage and special instrumentation[8].

In this study, we report a novel **"nano to nano" direct electrodeposition approach** for preparing nano-structured WO_3 films from WO_3 nanoparticle dispersion. This approach is based on the electrochemical reduction of WO_3 nanoparticles on the cathode. It combines the advantages of manipulating well-defined nanostructures in dispersion and the precise control of an electrodeposition process. WO_3 was selected as a model system due to the growing interest in this material for photocatalysis, electrochromism, *etc.*[6, 9-12] The electrodeposited WO_3 films, which consisted of crystalline nanoparticles of the same size as in the dispersion, exhibited extraordinary electrochromic performance of 92% contrast with 9 and 15 s of coloring and bleaching, respectively. Similarly, we also electrodeposited vanadium oxide nanobelts from its aqueous dispersion, and the results will be reported elsewhere. This approach of low voltage electrodeposition of nano-objects from dispersions is generic and applicable to a variety of other transition metal oxide systems.

Experimental

Materials: W powder (Merck), H_2O_2 (30%, Merck), $LiClO_4$ (96.9%, Sigma), propylene carbonate (BDH Chemicals) were used as recieved. All the chemicals used in this work were

reagent grade. DI water used in this work was 18.3 MΩ·cm purified from Barnstead Easypure UV system. The WO_3 dispersion for electrodeposition was synthesized by sol-gel method according to Costa *et al.*[13] ITO plates (CG-60IN-CUV, R_S=15-25 Ω, Delta Technologies Stillwater, MN) in the size of 0.7 × 2.5 cm^2 were cleaned by sequential sonication in ethanol, 1:1 $NH_3{\cdot}H_2O/H_2O_2$ (vol. ratio) and H_2O for 10, 30 and 10 min, respectively. After cleaning, the samples were blow-dried with N_2 flow before use. Ag grids (with a side length of 75 μm and line width of 3-4 μm) were fabricated on PET fabricated according to Layani *et al.*[14] with the use of silver dispersions with metal loading of 10 wt.%. A droplet of the dispersion was dripped on top of a stainless steel mesh (with opening of 40 μm and the mesh diameter of 16 μm, a gift from Micron, Germany) placed on the PET substrate. The liquid fills the gap between the mesh and substrates, and due to the wetting the silver nanoparticles align according to the wires of the mesh. At the end of solvent evaporation the mesh is removed, revealing a transparent grid composed of silver nanoparticles. The Ag grids adhere well to PET as evaluated by scotch tape test. The Ag grid/PET samples were cleaned with isopropanol prior to use.

Electrodeposition: Electrodeposition of the samples was carried out at room temperature (~25 °C) in a three-electrode compartment, with an Ag/AgBr quasi reference electrode (QRE, E = 390 ± 10 mV *vs.* ferrocene/ferrocene$^+$) and a graphite rod counter electrode. Electrodeposition was carried out by applying a constant negative potential to the ITO or Ag grid/PET sample, and the deposition current was recorded. The deposition solution consists of 5 wt.% nano-crystalline WO_3 dispersed in water without any other additive. The size of the WO_3 nanoparticles is 50-80 nm as characterized by SEM (**Figure 1C**). After electrodeposition, the samples were immediately withdrawn from the solution, carefully washed with ethanol and blow-dried with N_2 flow. The samples were kept in a Petri dish at room temperature (~25 ℃) for at least one night before characterization and electrochromic test, to remove the solvent and dry the films.

Electrochromic test: Electrochromic test was conducted in a three-electrode compartment. The test sample was connected as working electrode, a Ag wire was used as reference electrode and a Pt wire was used as counter electrode. All the three electrodes were placed in a glass cuvette. The potential of the sample was controlled by potentiostat, and the transmittance of the films was measured by a UV-vis spectrophotometer at wavelength of 350-800 nm. The cyclic coloring-bleaching test was done by applying −1.2 V (*vs.* Ag) for coloring, 0.4 V (*vs.* Ag) for bleaching on ITO samples, and -0.9 V (*vs.* Ag) for coloring, 0.3 V (*vs.* Ag) for bleaching on Ag grid/PET samples. Each coloring or bleaching segment was 120 s. The electrolyte was 1 mol/L $LiClO_4$ in propylenecarbonate. The test was performed at room temperature (~25 ℃).

Characterizations: The morphology of WO_3 films was characterized by scanning electron microscopy (SEM, SIRION, FEI Ltd.). The composition of the films was analyzed and mapped with Energy dispersive X-ray analysis (EDX, X-Max 20, Oxford Instruments, UK). X-ray diffraction (XRD) of the films was measured with D8 Advance diffractometer (Bruker Axs). The thickness of the films was measured by profilometer (P-15, KLA-Tencor Co., San Jose, CA). Scratch across the film was made by a wooden stick immediately after electrodeposition.

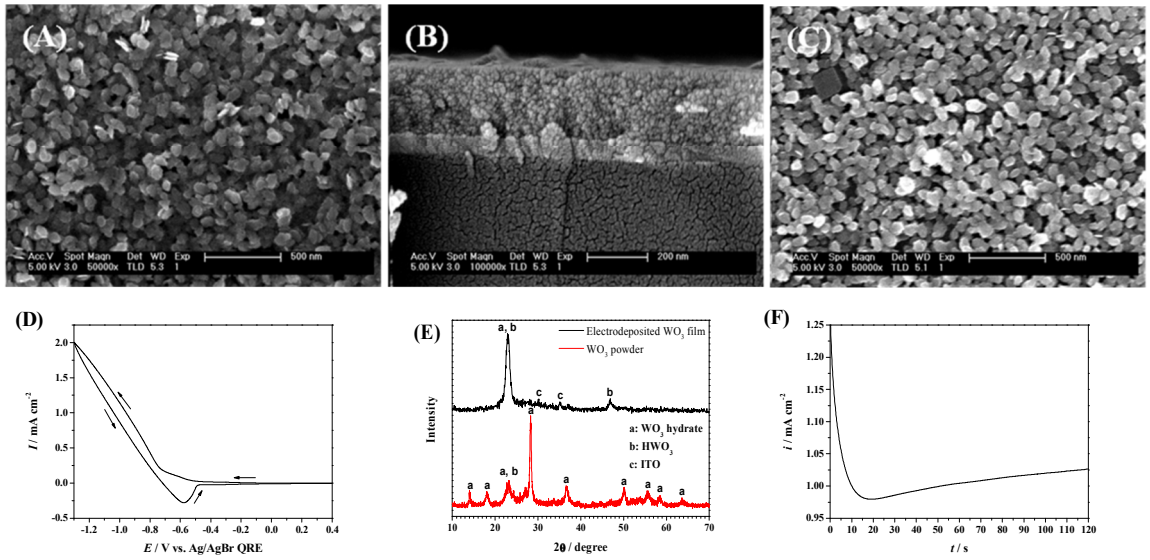

Fig. 1 XX SEM image of WO_3 film electrodeposited on ITO at −1.1 V (*vs.* Ag/AgBr QRE) for 100 s: (A) Top-view; (B) Cross-section. SEM image of WO_3 nanoparticles drop-casted on silicon wafer (C). Cyclic voltammetry of ITO in 5 wt.% WO_3 dispersion (D), scan rate: 50 mV/s. XRD patterns of WO_3 film electrodeposited on ITO at −1 V (*vs.* Ag/AgBr QRE) for 120 s and WO_3 nanoparticles drop-casted on Si wafer (E). Current response on ITO during electrodeposition at −1 V (*vs.* Ag/AgBr QRE) (F).

Results and Discussion

Figs. 1A-B show the top view and cross-section of a typical film electrodeposited on ITO by applying −1 V for 120 s *vs.* Ag/AgBr quasi reference electrode (QRE) in WO_3 nanoparticle dispersion. It is evident that the film consists of stacked nanoparticles where their shape and size are the same as in the dispersion, as shown from the SEM image of the WO_3 nanoparticles after drop-casting on a Si wafer (Fig. 1C). The size of the particles is between 50-80 nm. These results clearly indicate that electrodeposition successfully transfers the nanostructure from the dispersion to the film.

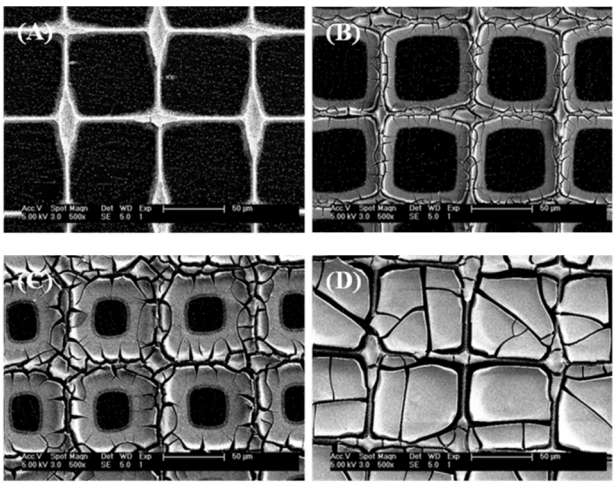

Fig. 2 SEM image of bare Ag grid/PET (A), WO_3 films electrodeposited on Ag grid/PET at −0.8 V (*vs.* Ag/AgBr QRE) for 3 min (B), 9 min (C) and 13 min (D).

The mechanism of nanoparticles deposition is of substantial importance for controlling the process. The WO_3 dispersion in this work is electrostatically stabilized as evidence by measuring the zeta potential (−51.8 mV in 0.5 wt.% dispersion). Therefore, the cathodic electrodeposition is not driven by electrophoretic migration as the nanoparticles are negatively charged, which may arise from the hydrated WO_4^{2-} groups on the surface of WO_3 nanoparticles[13]. Another possible mechanism involves charge neutralization due to pH change. Namely, during cathodic electrodeposition in aqueous media, the pH in the vicinity of the cathode may increase due to the reduction of O_2 or H_2O. This local pH change is known as a driving force for the **indirect** electrodeposition (electro-assisted deposition) of metal oxides or hydroxides (*e.g.* ZnO, $Ni(OH)_2$), latex nanoparticles and sol-gel films[15-19]. We found that WO_3 dispersion maintains its stability at pH 4 and precipitates after one hour at pH 8 (Supporting Information Fig. S1). Nevertheless, it is very unlikely that the electrodeposition of WO_3 nanoparticles is driven by pH increase. The interfacial pH near the cathode is almost impossible to significantly change during electrodeposition, as the bulk dispersion is highly acidic, *ca.* pH 1. Here, we consider that WO_3 nanoparticles deposit *via* **direct** electrochemical reduction. Cyclic voltammetry (Fig. 1D) shows that the reduction of WO_3 commences at −0.5 V *vs.* Ag/AgBr QRE, and a clear oxidation peak, which corresponds to the re-oxidation of the reduced WO_3 (HWO_3), is observed at the reverse scan. XRD pattern (Fig. 1E) of the dried WO_3 dispersion (yellow powder) matches that of WO_3 hydrate. On the other hand, the XRD analysis reveals that the electrodeposited WO_3 film mainly contains HWO_3. The latter is the product of the electrochemical reduction of WO_3 in water. The reduction of WO_3 is also seen from the blue color (known as "tungsten blue") of the as-deposited films, which gradually fades after films' exposure to air. The electrochemical reduction of WO_3 nanoparticles is described as follows and involves both the reduction of negatively hydrated WO_4^{2-} on the surface as well as bulk WO_3[4]:

$$WO_{4\,(surface)}^{2-} + 3H^+ + e^- \rightarrow HWO_{3(film)} + H_2O \qquad (1)$$

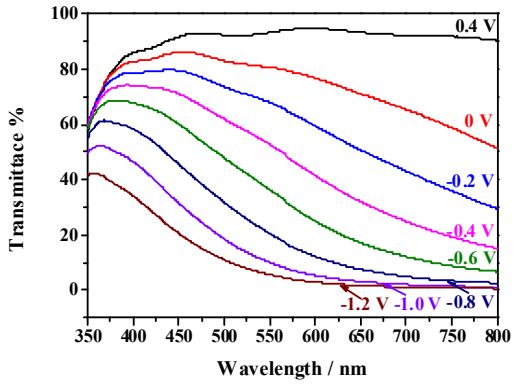

Fig. 3 Transmittance spectra of the WO_3 film electrodeposited at −1.1 V (*vs.* Ag/AgBr QRE) for 100 s on ITO. The spectra were measured at different potentials *vs.* Ag wire in propylene carbonate with 1 mol/L $LiClO_4$.

$$WO_{3(nanopartide)} + H^+ + e^- \rightarrow HWO_{3(film)} \qquad (2)$$

Upon reduction, the intercalated H^+ neutralizes the surface charge of WO_3 nanoparticles thereby causes film deposition. Since the reduced WO_3 is significantly more conductive than the oxidized form, it allows continuous film growth, which is indicated from the deposition current (Fig. 1F). Specifically, the current initially decreases, which is due to charging. After *ca.* 15 s, the deposition current gradually increases. This is attributed to the increasing conductive surface area caused by continuous WO_3 nanoparticles deposition.

The urge for replacing ITO as a major transparent conductive electrode is driven by the limited resources as well as by the development of printed electronics on flexible substrates[20]. Hence, we aimed also at applying our approach on Ag grids printed PET (denoted as Ag grid/PET). Fig. 2 shows the growth of WO_3 films on Ag grid/PET for different durations of deposition. Evidently, the film initially electrodeposits mostly on the Ag grid which is conductive. As deposition continues, the film grows on the grid laterally towards the center of the grid squares due to the high conductivity of reduced WO_3. Clearly, the film also thickens. After 13 min (-0.8 V vs. Ag/AgBr QRE) of deposition, the WO_3 film covers the entire PET surface (Fig. 2D). The film growth is further confirmed by EDX mapping of W signals (Supporting Information Fig. S2). These results indicate that the surface coverage of WO_3 films can be tuned by controlling the electrodeposition time. Notice that the latter required for coating the entire PET surface could be shortened by applying more negative potentials (Supporting Information Fig. S3). Moreover, the advantage of applying more negative potentials is not only in shortening the deposition time, but also in avoiding almost completely the formation of cracks as is shown in Fig. S3. Further experiments were therefore carried out at −1.1 V *vs.* Ag/AgBr QRE.

The essence of this approach lies in the "**nano to nano**" concept, whereby well-defined nano-objects dispersed in the liquid phase are electrodeposited to form nano-structured thin films. A major benefit of this method is maintaining the properties of the nano-objects in the deposited layer. This is nicely demonstrated by the excellent electrochromic performance of the electrodeposited

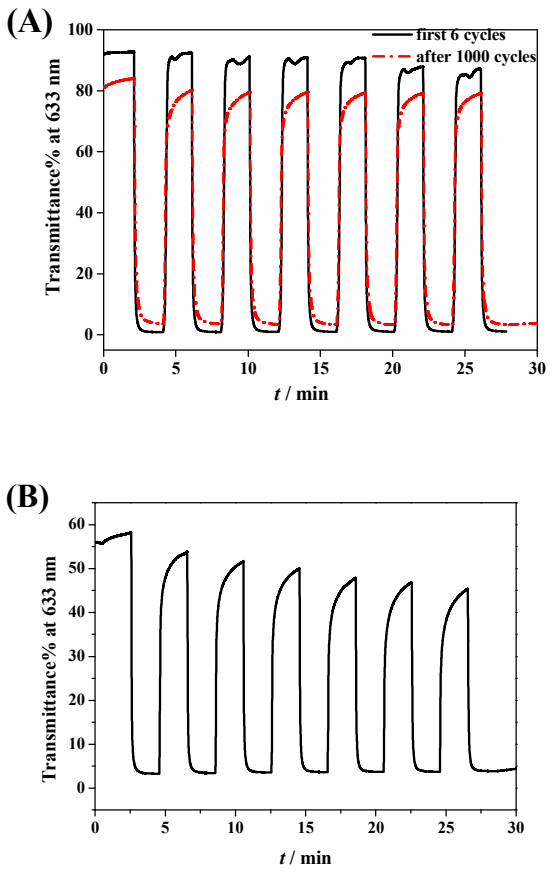

Fig. 4 Coloring-bleaching cycle test of WO_3 films electrodeposited at −1.1 V (vs. Ag/AgBr QRE) for 100 s on ITO and −1.15 V (vs. Ag/AgBr QRE) for 30 s on Ag grid/PET. Data were measured at 0.4 V (bleaching) and −1.2 V (coloring) *vs.* Ag wire in propylene carbonate with 1 mol/L $LiClO_4$.

nano-structured WO_3 films.

Fig. 3 shows the transmittance spectra of a WO_3 film electrodeposited on ITO. By applying 0.4 V (*vs.* Ag), the film is at full bleaching state and its transmittance is above 90% in the wavelength range of 400-800 nm. As the applied potential shifts negative, the film gradually turns blue and its transmittance decreases. The film becomes almost fully non-transparent at 600-800 nm when applying −1.0 and −1.2 V (*vs.* Ag). Furthermore, we tested the optical contrast variation of typical WO_3 films electrodeposited on ITO and Ag grid/PET during coloring-bleaching cycles. Contrast of *ca.* 92% (measured at 633 nm) is achieved with the optimized WO_3 film on ITO between full bleaching at 0.4 V and full coloring at −1.2 V (*vs.* Ag) (Fig. 4A), which is significantly higher than previously reported WO_3 films[10, 21, 22]. The coloring and bleaching times (to 90%) are 9 and 15 s, respectively. The coloration efficiency of this film is 51 cm^2/C as calculated from the first cycle (Supporting Information Fig. S4), which is comparable to other crystalline WO_3 films[23-25]. The coloring and bleaching are reversible, with *ca.* 76% contrast retaining after 1000 cycles. This suggests that the film has excellent long-term stability. The electrochromic test is demonstrated in Video S1. We recall that the electrodeposited WO_3 films consist of stacked nanoparticles as observed by SEM

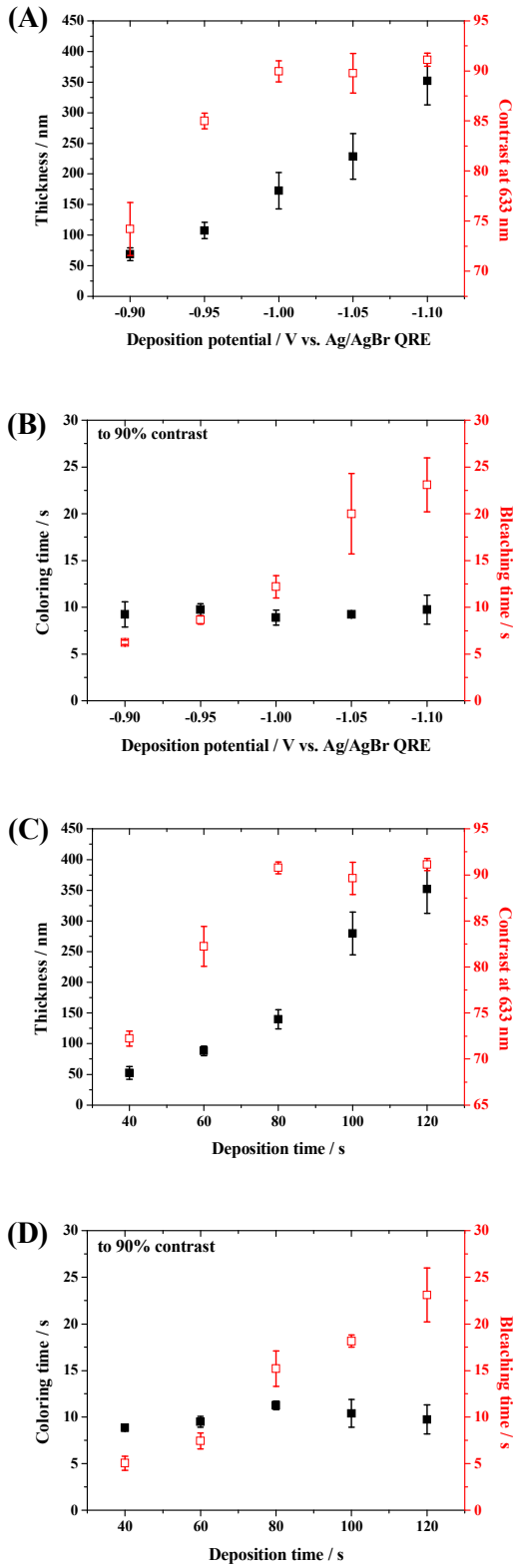

Fig. 5 Effect of deposition potential (A, B, t = 120 s) and time (C, D, E = −1.1 V *vs.* Ag/AgBr QRE) on the thickness, optical contrast (A, C), coloring time and bleaching time (B, D) of the electrodeposited WO_3 films.

(Figs. 1A-B). Hence, the porous morphology is highly permeable

towards the electrolyte and the nanostructure offers high active surface area. This explains the high contrast of the film. Moreover, the nanoparticles facilitate the intercalation and deintercalation of Li^+, yielding fast switching. The excellent long-term stability of the film may be attributed to the crystalline structure of the nanoparticles[23]. The detailed reasons for the pronounced enhancement in the films' electrochromic performance are discussed later.

The WO_3 film electrodeposited on Ag grid/PET from nanoparticle dispersion also exhibits high optical contrast (Fig. 4B). Considering that the native transmittance of Ag grid/PET substrate is only *ca.* 69%, the WO_3 film also switches between fully transparent and non-transparent states. Coloring of WO_3 film on Ag grid/PET takes 6.8 s (to 90%), which is shorter than the film on ITO. However, bleaching of the film on Ag grid/PET is substantially longer, and the transmittance of the film does not fully recover even after applying positive potential for 120 s. This phenomenon is attributed to the special assembly of Ag grids. During the coloring process, the coating on the grid is first reduced to $LiWO_3$ with intercalation of Li^+. Since $LiWO_3$ is conductive, it easily allows further coloring of the film deposited in between the grids. During the bleaching process, initially the film on the grid is oxidized back to WO_3 due to the high conductivity of the grid. However, different from coloring, the oxidized WO_3 is insulating, thus it introduces high resistance for further bleaching of the film in between the grids. This challenges the application of Ag grid/PET as transparent conductive electrode for electrochromic devices.

Electrodeposition of WO_3 films from its nanoparticle dispersion can be well-manipulated. Fig. 5 shows the variation of film thickness, contrast, coloring and bleaching times as a function of deposition potential and time. As the deposition potential becomes more negative and as the deposition time is longer, the thickness of the films increases, whereas the contrast of the films increases to a plateau of *ca.* 90-92% (Figs. 5A and 5C). This is already close to the maximum contrast possible on ITO since bare ITO in this work has a transmittance of *ca.* 95%. The coloring time is not significantly affected by the deposition parameters, whereas the bleaching time becomes longer as the film is thicker (Figs. 5B and 5D). This can be explained by the initial bleaching of the film/substrate interface, which leads to high interfacial resistance that inhibits bleaching of the outer layer of the film. The results indicate that the thickness and electrochromic performance of WO_3 films can be tuned by electrodeposition potential and time.

From the results above, it is clearly seen that nanocrystalline WO_3 films electrodeposited from WO_3 nanoparticle dispersion under optimal conditions have superior electrochromic performance as compared with the films prepared by other conventional methods. We recall that conventional electrodeposition methods using ionic WO_4^{2-} bath typically yield amorphous films without sintering, or crystalline films with large crystals after sintering at high temperature. The armophos films are integrate with low surface area. In order to increase the surface area and obtain nanostructures, surfactants are usually introduced. They are very difficult to be completely removed from the films after deposition, and the remained surfactants lower the conductivity thus deteriorate the electrochromic performance of the films. The amorphos films are also instable upon long-term cycling, due to the structure and volume change induced by intercalation/deintercalation of Li^+ ions. Sintering the films at high temperature may lead to crystalline structure that significantly improves stability. Yet, the large crystals hinder the deintercalation of Li^+ ions and therefore deteriorate the electrochromic performance of the films, especially the bleaching speed. Besides electrodeposition, WO_3 films can also be prepared by drop-casting, dip-coating, spin-coating or ink-jet printing. The drop-casted films are not homogenous and usually have poor adhesion to the substrate, while the latter three methods need to be applied repeatedly in order to obtain thick films with relatively high contrast[25]. The repeated coating processes are not only complicated but also yield high electrical resistance between consequently deposited layers, which limits the electrochromic performance. In comparison, the "nano to nano" electrodeposition route in this work yields unique nanostuctured films composed of stacked crystalline nanoparticles, offering **five** main advantages for electrochromism. **First,** the porous morphology as shown in **Figs. 1A-B** allows easy penetration of the electrolyte in the film, leading to the high active surface area. **Second,** the nanostructure facilitates the intercalation/deintercalation of Li^+ ions as compared with large crystals obtained by sintering. **Third,** the deposition precursor, *i.e.* a water dispersion of WO_3 crystalline nanoparticles stablized by electrostatic repulsion, is surfactant-free. This prevents the remain of surfactant in the film. **Fourth,** the growth mechanism of the films in electrodeposition, which is based on the high conductivity of reduced WO_3 nanoparticles, inherently ensures excellent electro-contact and low resistance between nanoparticles. This overcomes a major disadvantage of repeated dip-coating or spin-coating, which is the poor contact between consequently deposited layers. All the advantages above lead to extraordinary high contrast and fast color switching of the films. Besides these, the **fifth** advantage, which is the crystalline structure, yields high stablity in coloring-bleaching cycling as compared with the amorphos films (**Fig. 4A**). Moreover, the "nano to nano" electrodeposition approach is highly controllable. The thickness and electrochromic performance of the films can be easily tuned by deposition potential and time, as shown in **Fig. 5**.

Conclusions

WO_3 nanoparticles were successfully electrodeposited onto ITO and Ag grid/PET under mild potentials from their dispersion without adding surfactants or polymers. CV, current transient and XRD results reveal that the electrodeposition process is based on the electrochemical reduction of WO_3 nanoparticles. The reduction eliminates the electrostatic repulsion between nanoparticles, thus causes film deposition. Since the reduced WO_3 (HWO_3) is conductive, it allows further film growth. SEM images indicate that the electrodeposited films consist of stacked nanoparticles. This structure provides high active surface area, facilitates the penetration of electrolyte and the intercalation/deintercalation of Li^+ in the film and therefore results in outstanding electrochromic performance. The electrodeposition process can be manipulated by deposition parameters such as potential and time. On ITO, film can be tuned with different thickness and electrochromic properties while on

Ag grid/PET the surface coverage of WO_3 can be controlled. Optimized film on ITO has optical contrast of 92%, with 9 s coloring and 15 s bleaching (to 90%), and coloration efficiency of 51 cm^2/C. The film has high stability, with contrast retaining 76% after 1000 coloring/bleaching cycles. The film on Ag grid/PET also has excellent contrast and coloring speed, but the bleaching time is very long due to the grid assembly. This work offers a novel "nano to nano" electrodeposition approach based on the electrochemical redox of nano-objects, which can be extended to various transition metal oxides with different size and shape.

Acknowledgements

This work was supported by NTU-HUJ-BGU Nanomaterials for Energy and Water Management Programme under the Campus for Research Excellence and Technological Enterprise (CREATE), that is supported by the National Research Foundation, Prime Minister's Office, Singapore. The Harvey M. Krueger Family Center for Nanoscience and Nanotechnology of the Hebrew University is also acknowledged.

Notes and references

[a] *Institute of Chemistry, The Hebrew University of Jerusalem, Jerusalem 9190401, Israel. Fax: 972 2 6585319; Tel: 972 2 6585831; E-mail: Daniel.mandler@mail.huji.ac.il, Magdassi@mail.huji.ac.il*

[b] *School of Materials Science and Engineering, Nanyang Technological University, Singapore 639798, Singapore.*

† Electronic Supplementary Information (ESI) available: [Photos of 5 wt.% WO_3 dispersion at different pH, EDX mapping of W for the WO_3 films electrodeposited on Ag grid/PET at −0.8 V (*vs.* Ag/AgBr QRE) for different time, SEM/EDX mapping of W for the WO_3 films electrodeposited on Ag grid/PET at −1.1 V (*vs.* Ag/AgBr QRE) for 30 s, coloration efficiency of WO_3 films electrodeposited at −1.1 V (*vs.* Ag/AgBr QRE) for 100 s on ITO, video demonstration of coloring and bleaching of the optimal nano-crystalline WO_3 film electrodeposited on ITO.]. See DOI: 10.1039/b000000x/

‡ Liang Liu and Michael Layani contributed equally to this work.

1. C. Burda, X. Chen, R. Narayanan and M. A. El-Sayed, *Chem. Rev.*, 2005, **105**, 1025-1102.
2. Y. Xia, P. Yang, Y. Sun, Y. Wu, B. Mayers, B. Gates, Y. Yin, F. Kim and H. Yan, *Adv. Mater.*, 2003, **15**, 353-389.
3. G. H. A. Therese and P. V. Kamath, *Chem. Mater.*, 2000, **12**, 1195-1204.
4. E. A. Meulenkamp, *J. Electrochem. Soc.*, 1997, **144**, 1664-1671.
5. N. Kanani, *Electroplating: Basic Principles, Processes and Practice*, Elsevier, Oxford, UK, 2004.
6. S. H. Baeck, K. S. Choi, T. F. Jaramillo, G. D. Stucky and E. W. McFarland, *Adv. Mater.*, 2003, **15**, 1269-1273.
7. R. M. Penner, *J. Phys. Chem. B*, 2002, **106**, 3339-3353.
8. J. H. B. Dickerson, Aldo R. (Eds.), *Electrophoretic Deposition of Nanomaterials*, Springer, 2012.
9. M. A. Butler, *J. Appl. Phys.*, 1977, **48**, 1914-1920.
10. G. A. Niklasson and C. G. Granqvist, *J. Mater. Chem.*, 2007, **17**, 127-156.
11. S.-H. Lee, H. M. Cheong, P. Liu, D. Smith, C. E. Tracy, A. Mascanrenhas, J. R. Pitts and S. K. Deb, *Journal of Applied Physics*, 2000, **88**, 3076-3078.
12. J. Z. Ou, S. Balendhran, M. R. Field, D. G. McCulloch, A. S. Zoolfakar, R. A. Rani, S. Zhuiykov, A. P. O'Mullane and K. Kalantar-zadeh, *Nanoscale*, 2012, **4**, 5980-5988.
13. C. Costa, C. Pinheiro, I. Henriques and C. A. T. Laia, *ACS Appl. Mater. Interf.*, 2012, **4**, 1330-1340.
14. M. Layani and S. Magdassi, *J. Mater. Chem.*, 2011, **21**, 15378-15382.
15. S. Peulon and D. Lincot, *Adv. Mater.*, 1996, **8**, 166-170.
16. S. Peulon and D. Lincot, *J. Electrochem. Soc.*, 1998, **145**, 864-874.
17. L. Indira and P. V. Kamath, *J. Mater. Chem.*, 1994, **4**, 1487-1490.
18. I. Levy, S. Magdassi and D. Mandler, *Electrochim. Acta*, 2010, **55**, 8590-8594.
19. R. Shacham, D. Avnir and D. Mandler, *Adv. Mater.*, 1999, **11**, 384-388.
20. D. S. Hecht, L. Hu and G. Irvin, *Adv. Mater.*, 2011, **23**, 1482-1513.
21. W. Cheng, E. Baudrin, B. Dunn and J. I. Zink, *J. Mater. Chem.*, 2001, **11**, 92-97.
22. K. Wang, P. Zeng, J. Zhai and Q. Liu, *Electrochemistry Communications*, 2013, **26**, 5-9.
23. S. H. Lee, R. Deshpande, P. A. Parilla, K. M. Jones, B. To, A. H. Mahan and A. C. Dillon, *Advanced Materials*, 2006, **18**, 763-766.
24. J. Wang, E. Khoo, P. S. Lee and J. Ma, *The Journal of Physical Chemistry C*, 2009, **113**, 9655-9658.
25. M. Layani, P. Darmawan, W. L. Foo, L. Liu, A. Kamyshny, D. Mandler, S. Magdassi and P. S. Lee, *Nanoscale*, 2014, **6**, 4572-4576.